PROCEEDINGS OF SCIENCE

Towards Lamb shift spectroscopy of antihydrogen atoms at the GBAR $\bar{\mathrm{H}}$ beam line

T. A. Tanaka,[a,*] P. Blumer,[b] G. Janka,[c] B. Ohayon,[d] C. Regenfus,[b] P. Crivelli,[b] N. Kuroda,[a] on behalf of the GBAR collaboration, R. Tsukida,[a] T. Higuchi[e] and K. S. Tanaka[f]

[a] *Institute of Physics, The University of Tokyo, Komaba, Meguro-ku 153-8902, Tokyo, Japan*
[b] *Institute for Particle Physics and Astrophysics, ETH Zürich, Otto-Stern-Weg, Zürich 8093, Switzerland*
[c] *PSI Center for Neutron and Muon Sciences CNM, 5232 Villigen PSI, Switzerland*
[d] *The Helen Diller Quantum Center, Department of Physics, Technion-Israel Institute of Technology, Haifa 3200003, Israel*
[e] *Institute for Integrated Radiation and Nuclear Science (KURNS), Kyoto University, Asashiro-nishi, Kumatori-cho 590-0494, Osaka, Japan*
[f] *Research Institute for Science and Engineering (RISE), Waseda University, Okubo, Shinjuku-ku 169-0072, Tokyo, Japan*

E-mail: takumi05@radphys4.c.u-tokyo.ac.jp

A microwave (MW) spectroscopy experiment has been proposed to directly measure the resonant frequency of $2S_{1/2} - 2P_{1/2}$ Lamb shift transition in antihydrogen ($\overline{\mathrm{H}}$) atoms. The spectroscopy opens up the possibility of deriving the charge radius of antiproton ($\bar{\mathrm{p}}$) using a beam of $\overline{\mathrm{H}}$ atoms with a kinetic energy of a few keV travelling in a magnetic field-free environment. The requisite spectroscopy apparatuses have been developed and installed in the $\overline{\mathrm{H}}$ beam line at the GBAR experiment, where the production of $\overline{\mathrm{H}}$ beam at 6.1 keV was demonstrated through a charge exchange reaction of a $\bar{\mathrm{p}}$ beam passing through a positronium (Ps) cloud. The spectroscopy setup is composed of a MW spectrometer and a Lyman-α photon detector. The MW spectrometer consists of two consecutive MW apparatuses which have a relatively large borehole of 30 mm diameter, and each MW apparatus comprises a pair of parallel plate electrodes as its inner conductor and a rectangular box as its outer conductor. Downstream to the MW spectrometer, the Lyman-α detector has been installed to count the $\overline{\mathrm{H}}$ atoms remaining in the $2S$ state after interacting with the MW E-field. Towards the $\overline{\mathrm{H}}$ Lamb shift spectroscopy, we present here a characterization of the MW spectrometer, an evaluation of the detection efficiency of the Lyman-α detector, and a precision expected in the first line shape measurement of the $\overline{\mathrm{H}}$ Lamb shift.

International Conference on Exotic Atoms and Related Topics and Conference on Low Energy Antiprotons (EXA-LEAP2024)
26-30 August 2024
Austrian Academy of Sciences, Vienna.

*Speaker

 ISSN 1824-8039 . Published by SISSA Medialab.

PoS(EXA-LEAP2024)044

1. Introduction

The Lamb shift in hydrogen (H) atom is a 1 GHz energy difference between the $2S_{1/2}$ and $2P_{1/2}$ states due to the effects of quantum electrodynamics (QED) [1]. The leading order of the contribution originating from the finite nuclear size effect in the H atom relates to the root-mean-square of charge distribution in the proton, i.e., the proton charge radius (PCR). Along with the progress of spectroscopic techniques with MW technology, high-precision measurements of the $2S_{1/2} - 2P_{1/2}$ Lamb shift in H atoms have derived the PCR [2, 3]. The most precise MW spectroscopy of the Lamb shift in H atoms achieves a precision of 3 ppm, with the PCR determined to an accuracy of 1% [4].

A direct MW spectroscopy of the Lamb shift in antihydrogen ($\overline{\mathrm{H}}$) atoms has not yet been attempted, i.e., the charge radius of antiproton ($\bar{\mathrm{p}}$) has not yet been experimentally investigated, while the ALPHA collaboration has indirectly measured the Lamb shift of $\overline{\mathrm{H}}$ atoms with 10% precision with a technique of laser spectroscopy in a high magnetic field environment [5].

The GBAR (Gravitational Behaviour of Anti-hydrogen at Rest) experiment, running in the AD/ELENA facility at CERN, aims at a precise measurement of the free fall acceleration of $\overline{\mathrm{H}}$ atoms using antihydrogen ions ($\bar{\mathrm{H}}^+$) produced through the following two-stage charge-exchange reactions with positronium (Ps) atoms — a bound state of e^- and e^+ — [6]:

$$\bar{\mathrm{p}} + \mathrm{Ps} \longrightarrow \overline{\mathrm{H}} + e^- \tag{1}$$

$$\overline{\mathrm{H}} + \mathrm{Ps} \longrightarrow \bar{\mathrm{H}}^+ + e^- \tag{2}$$

They have recently succeeded in producing beam-like $\overline{\mathrm{H}}$ atoms at the first stage of the reactions, using the $\bar{\mathrm{p}}$ beam with a kinetic energy of 6.1 keV passing through a cloud of Ps atoms [7]. Under this production scheme, theoretical calculations predict the presence of $2S$ state $\overline{\mathrm{H}}$ atoms [8].

In this context, a direct measurement of the Lamb shift in $\overline{\mathrm{H}}$ atoms has been proposed, utilizing the $2S$ state $\overline{\mathrm{H}}$ atoms in a magnetic field-free environment in the GBAR $\overline{\mathrm{H}}$ beam line [9, 10].

2. Experimental scheme

Figure 1 shows allowed transitions in $n = 2$ Lamb shift levels with a linearly polarized E-field of MW. Here, the quantum number F denotes the total angular momentum of the atom and m_F for its total magnetic quantum number. Figure 2 shows the schematic view of the Lamb shift spectroscopy experiment in the GBAR beam line. The $\overline{\mathrm{H}}$ atom produced via the first charge exchange reaction (Eq. 1) is represented by the green arrow. The MW spectrometer consists of two consecutive MW apparatuses, *Hyperfine Selector* (HFS) and *Microwave Scanner* (MWS), to simplify the line shape of the hyperfine states in Lamb shift levels. The HFS filters out the $2S_{1/2}$ ($F = 1$) states, resonant at 1088 MHz and 1147 MHz, by irradiating a MW at a fixed frequency of 1.1 GHz. Then, the MWS irradiates a MW of a specific frequency ranging from 0.6 GHz to 1.5 GHz for the $\overline{\mathrm{H}}$ atoms. Downstream of the MW spectrometer, the number of remaining $\overline{\mathrm{H}}(2S_{1/2})$ atoms is counted in the Lyman-α detector. As a consequence of using both the HFS and MWS, the single peak spectrum of the $2S_{1/2}$ ($F = 0, m_F = 0$) state resonant at 910 MHz can be obtained. The detailed description is given in Ref. [11]. Similar methods have been adopted in the Lamb shift spectroscopy of H atoms [2–4].

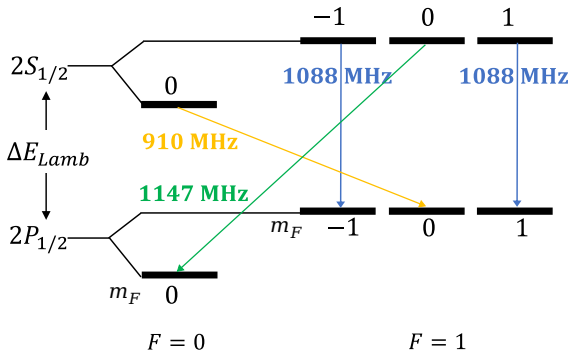

Figure 1: Allowed transitions in $n = 2$ Lamb shift of (anti-)hydrogen atom with linearly polarized MW.

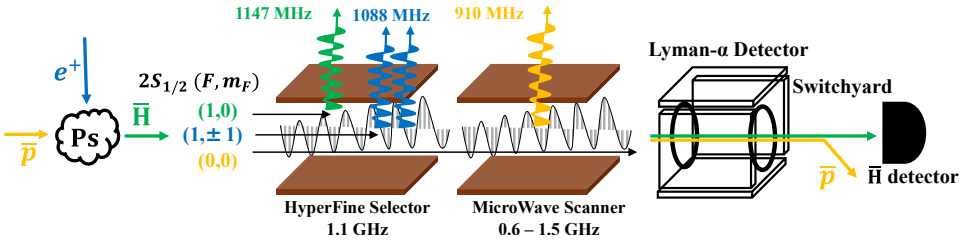

Figure 2: Lamb shift spectroscopy setup in the GBAR experiment.

The Lyman-α detector consists of two ring electrodes to form a DC electric field (DC E-field) and CsI coated microchannel plates (MCPs) [12]. The remaining $\bar{\mathrm{H}}(2S_{1/2})$ atoms are counted by deexciting them to the ground state through the Lyman-α transition via Stark mixing and detecting the Lyman-α photons using the CsI MCPs.

Downstream to the Lyman-α detector, an electrostatic switchyard to deflect $\bar{\mathrm{p}}$ is situated, followed by a $\bar{\mathrm{H}}$ detector comprising a MCP, a phosphor screen, and a CCD camera. The signal here will be used to take the coincidence with the signal in the Lyman-α detector.

3. Characterization of the MW spectrometer

A schematic view of the MW apparatus and the circuit components are shown in Fig. 3. The apparatus is composed of a pair of parallel plate electrodes and a rectangular box [13], inspired by apparatuses used in the hydrogen Lamb shift spectroscopy [3]. The Lamb shift spectroscopy of muonium (Mu) atoms has been performed using a similar MW apparatuses with the borehole diameter of 20 mm and similar circuit components [13–15]. Also, the H Lamb shift measurement was demonstrated in the GBAR beam line employing a proton gun and a carbon foil [16].

Towards the $\bar{\mathrm{H}}$ Lamb shift spectroscopy, the MW apparatuses with a larger borehole diameter of 30 mm were developed in order to reduce the loss of the $\bar{\mathrm{H}}$ or $\bar{\mathrm{p}}$ beams at the MW apparatuses [11]. The geometry was optimized for both the HFS and MWS to gain the MW E-field amplitude even with the larger separation of the upper and lower electrodes. Furthermore, the HFS was designed to resonate at the fixed frequency of 1.1 GHz, enhancing the MW E-field amplitude and efficiently removing the $2S_{1/2}(F = 1)$ state.

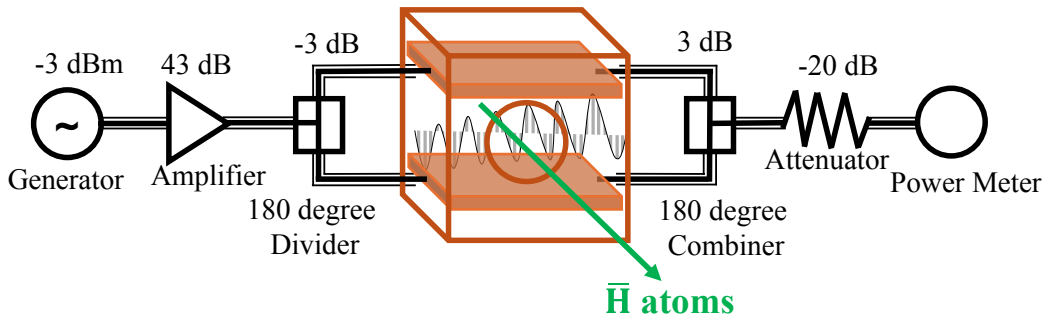

Figure 3: Structure of MW apparatus and the associated MW circuit components.

The MW signal is produced by a signal generator at 0.5 mW and amplified to 10 W by a Mini-Circuits ZHL-10W-2G+ amplifier with a typical gain of 43 dB. The amplified signal is then split by a 180-degree phase-inverting high power divider (TRM HS101fc900). This setup enables the highest signal transmission around the resonant frequency for the $2S_{1/2}$ ($F = 0$, $m_F = 0$) state. The phase-inverted signals are fed to the upper and lower electrodes of the apparatus to form an oscillating E-field between the electrodes to interact with the $\overline{\mathrm{H}}(2S_{1/2})$. The MW signals passing through the MW apparatus are combined and attenuated, and the power is measured at the end.

The total input powers into the MW apparatuses were evaluated in situ by correcting the value monitored at the power meter using the S-parameters of the circuit components, which had been measured in advance by a vector network analyzer. Figure 4 shows the spectra of the total input powers when the signal generator outputs −3 dBm (0.5 mW).

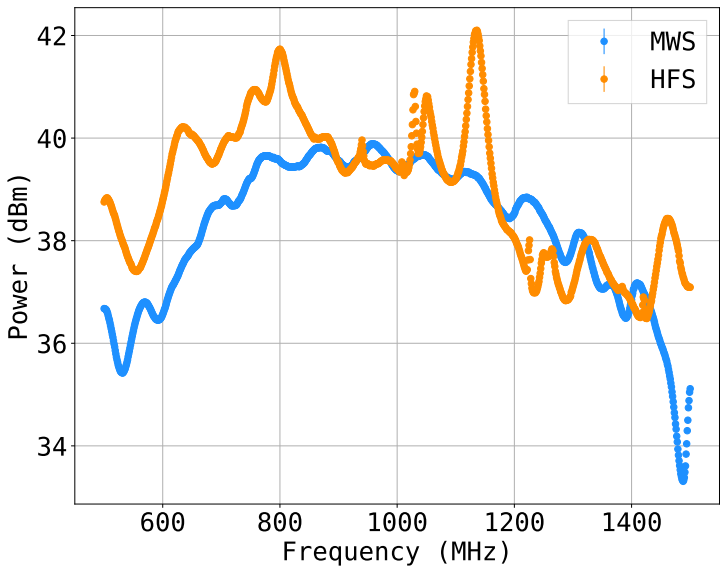

Figure 4: Measured MW powers at the entrance of the HFS and MWS when the output power of the signal generator was set to −3 dBm.

The total input power on the MWS is more than 37 dBm (5 W) from 700 MHz to 1300 MHz

and the spectrum peaks around 900 MHz. A part of this dependency is due to the frequency characteristic of the high power divider. Another part of the dependency is due to the characteristic of the amplifier, which guarantees the typical gain of 43 dB in the range from 800 MHz to 2000 GHz. For the HFS, the total input power peaks at 1135 MHz, which is considered due to the resonant property designed around 1.1 GHz.

Concerning the temporal stability of the MW power, the measured power value was observed to decrease by approximately 1% over a few minutes before reaching a plateau. For the planned spectroscopy experiment, the power drift will be monitored to account for the associated systematic uncertainty.

4. Detection efficiency of the Lyman-α detector

The detection efficiency of the MCP of the Lyman-α detector itself was characterized as 22(2)%, including the quantum efficiency of the CsI coated on the surface [12, 17]. The geometrical acceptance of the MCPs, taking into account the spatial distribution of the $\overline{\mathrm{H}}$ beam and the DC E-field to quench the $\overline{\mathrm{H}}(2S_{1/2})$, was re-evaluated to compute the overall detection efficiency of the detector in the planned $\overline{\mathrm{H}}$ Lamb shift spectroscopy.

In the $\overline{\mathrm{H}}$ production experiment in 2022, the 100 keV $\bar{\mathrm{p}}$ beam from ELENA was slowed down to 6.1 keV by the drift tube type decelerator. The beam transmission efficiency from the Ps target to the $\overline{\mathrm{H}}$ detector was evaluated by SIMION simulations to be 68% as an upper limit for the $\overline{\mathrm{H}}$ and 74% for the $\bar{\mathrm{p}}$, respectively [7]. The trajectories of the $\overline{\mathrm{H}}$ atoms are calculated to evaluate the detection efficiency of the Lyman-α detector, which reproduces the transmission efficiency of 68%.

For the DC E-field formed by the two ring electrodes, we have been testing a scheme to keep the upstream electrode grounded and apply a high voltage only to the downstream electrode to have a higher geometrical acceptance of the MCPs for the emitted Lyman-α photons than the case where an anti-symmetric set of voltages is applied on the electrodes.

Figure 5 illustrates the map of the DC E-field when 3 kV is applied to the downstream electrode. An example of the trajectory of the $\overline{\mathrm{H}}$ atom flying from the left and the trajectory of the Lyman-α photon are represented as the black and green lines, respectively. The MCPs are represented as the red plates, and the hit point of the photon on the MCP is shown as the blue cross. As shown in Fig. 6, Monte Carlo simulations have verified that the geometrical acceptance keeps increasing as the higher voltage is applied to the downstream electrode. Almost all $2S$ state $\overline{\mathrm{H}}$ is deexcited above 2.5 kV, and more than 30% of emitted Lyman-α photons are accepted by the CsI MCPs.

When 3 kV is applied to the downstream ring, the total detection efficiency can be estimated to be around 7% by multiplying the geometrical acceptance and the detection efficiency of the MCP.

5. Simulation of the resonant line shape

Monte Carlo simulations were performed along the calculated trajectories of $\overline{\mathrm{H}}$ atoms to estimate the period of measurement needed to achieve a certain precision of the spectroscopy. The Lamb shift transition was described by integrating the time-dependent Schrödinger equation, including the obtained characteristics of the MW apparatuses. The Stark mixing in the Lyman-α detector was also modeled to estimate the probability of Lyman-α photon emission. The detected

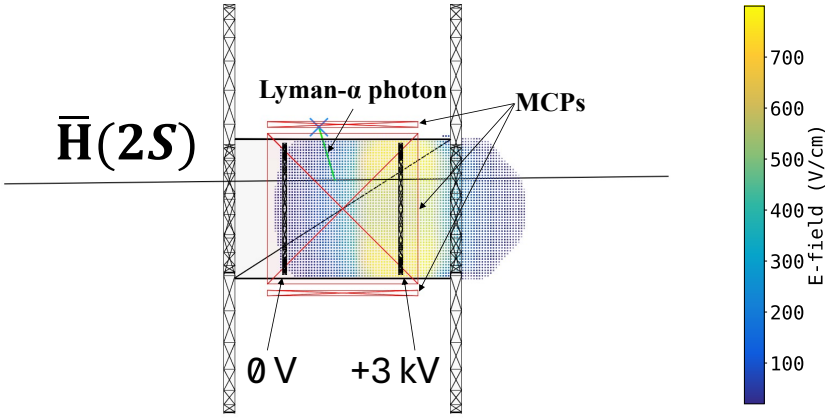

Figure 5: A map of the E-field formed by Lyman-α detector and an example of emitted Lyman-α photon.

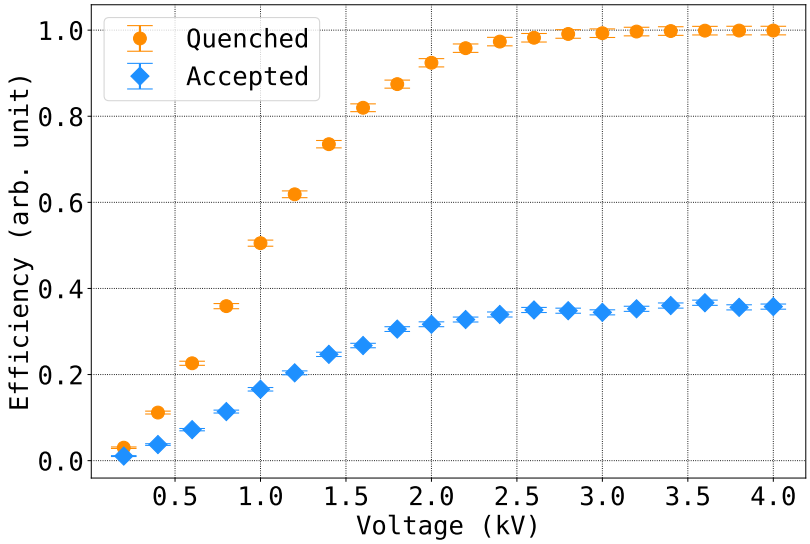

Figure 6: Calculated ratio of the deexcited $2S$ state (orange-filled circle) and the calculated detectable fraction (blue-filled rectangle) against the applied voltage on the downstream ring of the Ly-α detector.

number of Lyman-α photons was then obtained for each frequency from the geometrical acceptance and the efficiency of the detector. Thus, the resonant line shape was simulated.

In the first spectroscopic measurement, the MWS will be used to obtain a spectrum containing all possible transitions indicated in Fig. 1 rather than a state-selected spectrum. Here, we assume the production rate of 0.1 $\overline{\mathrm{H}}$ atoms and the ratio of 10% in $2S_{1/2}$ state [8], expected to be achieved in the GBAR $\overline{\mathrm{H}}$ line in 2024. Assuming a few months of the data-taking campaign with 120 s of the mixing cycle and 80% of the duty cycle of the AD/ELENA facility, a spectrum of the Lyman-α photon counts is expected as shown in Fig. 7. At each frequency, 300 $\overline{\mathrm{H}}(2S_{1/2})$ are simulated, and 5 W is input to the MWS.

To fit the spectrum contributed by all sublevels of the $2S_{1/2}$ state, i.e., $(F, m_F) = (0,0), (1,0),$

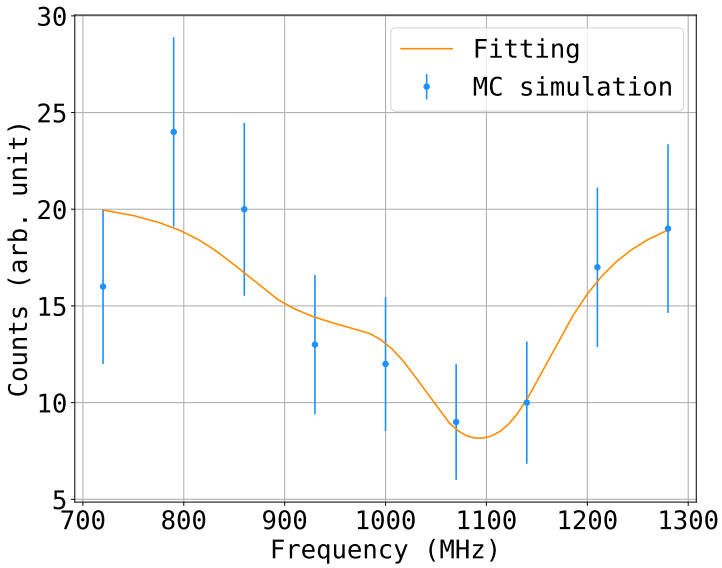

Figure 7: Monte Carlo simulation of the Lamb shift spectrum and fit to the simulation, assuming a few months of the spectroscopic measurement with the total MW power of 5 W input to the MWS.

and $(1, \pm 1)$, three Lorentz functions are simply adopted. The fitting results reach a precision of 10% to determine the Lamb shift. This will be the first direct measurement of the comparable precision achieved in the precedent indirect measurement [5].

6. Conclusion and Perspective

A direct spectroscopic measurement of the Lamb shift in $\overline{\mathrm{H}}$ atoms has been planned in the GBAR experiment. The frequency dependencies of the MW power at the entrance of the apparatuses have been characterized, and the detection efficiency of the Lyman-α detector has been evaluated. The Monte Carlo simulation predicts that a few months of data taking would reach the spectroscopy precision of 10% with the expected $\overline{\mathrm{H}}$ beam intensity in the coming year.

The background for the Lyman-α detector has been examined with $\bar{\mathrm{p}}$ beams in the 2024 beam time, and analysis is ongoing. In the following years, the improved production rate of 0.1 $\overline{\mathrm{H}}$ atoms per AD/ELENA cycle, which is one order of magnitude higher than the results in 2022, is foreseen. The first measurement should confirm $2S$ state $\overline{\mathrm{H}}$ atoms by detecting Lyman-α photons by switching the MW frequency on and off, followed by the first line shape measurement.

References

[1] V.A. Yerokhin et al., *Theory of the lamb shift in hydrogen and light hydrogen-like ions*, *Annalen der Physik* **531**, 1800324 (2019)

[2] G. Newton et al., *A precision determination of the Lamb shift in hydrogen*, *Philos. Trans. R. Soc. A*, **290**, 35 (1979)

[3] S. R. Lundeen and F. Pipkin, *Separated oscillatory field measurement of the lamb shift in H, n = 2*, *Metrologia* **22**, 9 (1986)

[4] N. Bezginov et al., *A measurement of the atomic hydrogen Lamb shift and the proton charge radius*, *Science*, **365**, 1007 (2019)

[5] M. Ahmadi et al., *Investigation of the fine structure of antihydrogen*, *Nature* **578**, 375-380 (2020)

[6] P. Perez et al., *The GBAR antimatter gravity experiment*, *Hyperfine Interact.*, **233**, 21 (2015)

[7] P. Adrich et al., *Production of antihydrogen atoms by 6 keV antiprotons through a positronium cloud*, *Eur. Phys. J. C*, **83**, 1004 (2023)

[8] C. M. Rawlins et al., *Calculation of antihydrogen formation via antiproton scattering with excited positronium*, *Phys. Rev. A* **93**, 012709 (2016)

[9] P. Crivelli et al., *Antiproton charge radius*, *Phys. Rev. D*, **94**, 052008 (2016)

[10] N. Kuroda, et al., *Lamb shift measurement of antihydrogen for determining the charge radius of antiproton and a stringent test of CPT symmetry*, *J. Phys. Conf. Ser.*, **875**, 022054 (2017)

[11] T. A. Tanaka et al., *Design of a microwave spectrometer for high-precision Lamb shift spectroscopy of antihydrogen atoms*, *Interactions*, *245*:30 (2024)

[12] G. Janka et al., *Intense beam of metastable Muonium.*, *Eur. Phys. J. C.* **80**, 804, (2020)

[13] G. Janka, Ph.D. Thesis, ETH Zürich (2022)

[14] B. Ohayon et al., *Precision measurement of the Lamb shift in muonium*, *Phys. Rev. Lett.* **128**, 011802 (2022)

[15] G. Janka et al., *Measurement of the transition frequency from* $2S_{1/2}$*,* $F = 0$ *to* $2P_{1/2}$*,* $F = 1$ *states in muonium*, *Nat. Commun.* **13**, 7273 (2022)

[16] GBAR Collaboration, CERN-SPSC-2022-003/SPSC-SR-302, (2022)

[17] A.S. Tremsin and O.H.W. Siegmun, *Dependence of quantum efficiency of alkali halide photocathodes on the radiation incidence angle*, *Proc. SPIE* **3765**, 441 (1996)

Acknowledgments

The authors are grateful to the GBAR collaboration for their support. This work has been supported by Yamada Science Foundation, JSPS KAKENHI Grant-in-Aid for Scientific Research A 20H00150, and Fostering Joint International Research A 20KK0305 (Japan), the ERC consolidator grant 818053-Mu-MASS, the Swiss National Science Foundation under the grants 197346/201465 and the ETH grant 46-17-1. T.A.T. is supported by JST SPRING JPMJSP2108 and the Murata Science Foundation. B.O. acknowledges support from the European Union's Horizon 2020 research and innovation program under the Marie Skłodowska-Curie grant agreement No. 101019414, as well as ETH Zurich through a Career Seed Grant SEED-09 20-1.